Haroun et al. *Boundary Value Problems* (2015) 2015:161
DOI 10.1186/s13661-015-0424-3

Boundary Value Problems
a SpringerOpen Journal

RESEARCH Open Access

Heat and mass transfer of nanofluid through an impulsively vertical stretching surface using the spectral relaxation method

Nageeb AH Haroun[1], Precious Sibanda[1], Sabyasachi Mondal[1*], Sandile S Motsa[1] and Mohammad M Rashidi[2]

*Correspondence:
sabya.mondal.2007@gmail.com
[1]School of Mathematics, Statistics and Computer Science, University of KwaZulu-Natal, Private Bag X01, Scottsville, Pietermaritzburg, 3209, South Africa
Full list of author information is available at the end of the article

Abstract

In this paper, we investigate heat and mass transfer in a magnetohydrodynamic nanofluid flow due to an impulsively started stretching surface. The flow is subject to a heat source, a chemical reaction, Brownian motion and thermophoretic parameters which are assumed to be significant. We have further assumed that the nanoparticle volume fraction at the wall may be actively controlled. The physical problem is modeled using systems of nonlinear differential equations which have been solved numerically using the spectral relaxation method. Comparing with previously published results by Khan and Pop (Int. J. Heat Mass Transf. 53:2477-2483, 2010) shows an excellent agreement. Some of the particular findings are that the skin friction coefficient decreases with an increase in the nanoparticle volume fraction, the heat transfer coefficient decreases with an increase in the nanoparticle volume fraction and that the mass transfer coefficient increases with an increase in the nanoparticle volume fraction.

Keywords: nanofluids; impulsively stretching surface; magnetohydrodynamic; chemical reaction parameter; spectral relaxation method

1 Introduction

The term nanofluid denotes a liquid in which nanoscale particles are suspended in a base fluid with low thermal conductivity such as water, oils and ethylene glycol. In recent years, the concept of nanofluid has been proposed as a route for increasing the performance of heat transfer liquids. Due to the increasing importance of nanofluids, there is now a large amount of literature on convective transport of nanofluids and problems linked to a stretching surface. Choi [1] initially pointed out that addition of these nanoparticles to the base fluid appreciably enhances the effective thermal conductivity of the fluid. An excellent collection of articles on this topic can be found in [2, 3] and Das *et al.* [4]. A non-homogenous equilibrium model proposed by Buongiorno [5] revealed that the massive increase in the thermal conductivity occurs due to the presence of two main effects; namely the Brownian diffusion and the thermophoretic diffusion of nanoparticles. The study of a steady boundary layer flow of a nanofluid towards a stretching sheet was reported by Khan and Pop [6]. Radiation effects on the viscous flow of a nanofluid and heat transfer over a nonlinearly stretching sheet were studied by Hady *et al.* [7]. Kuznetsov and Nield

[8] carried out a numerical investigation of mixed convection in the nanofluid flow over a vertical flat plate. In related work, Nield and Kuznetsov [9] studied the Cheng-Minkowycz problem for the natural convection in nanofluid flow over a flat plate. Yacob *et al.* [10] studied the stagnation point flow of a nanofluid flow due to a stretching/shrinking sheet using a shooting technique together with a fourth-fifth order Runge-Kutta method. Recently, results of MHD mixed convection in unsteady nanofluid flow due to a stretching/shrinking surface with suction/injection were reported by Haroun *et al.* [11]. In this study the model equations were solved using a spectral relaxation method. Stagnation point flow of a nanofluid with heat generation/absorption and suction/blowing was investigated by Hamad and Ferdows [12]. Rashidi and Erfani [13] used the modified differential transform method to investigate boundary layer flow due to stretching surfaces. Some excellent articles on the flow of nanofluids include those by Rashidi *et al.* [14], Anwar Bég *et al.* [15] and Garoosi *et al.* [16]. Some interesting results on discrete problems were presented by [17, 18].

Magnetohydrodynamic (MHD) flow and heat and mass transfer over a stretching surface have many important technological and industrial applications such as in micro MHD pumps, micro mixing of physiological samples, biological transportation and in drug delivery. An excellent collection of articles on this topic can be found in [19, 20]. The application of magnetic field produces a Lorentz force which assists in mixing processes as an active micromixing technology technique. Hence, transportation of conductive biological fluids in micro systems may greatly benefit from theoretical research in this area (see Yazdi *et al.* [21]). Studies on magneto-hydrodynamics (MHD) free convective boundary layer flow of nanofluids are very limited. More recently, Chamkha and Aly [22] studied magneto-hydrodynamics (MHD) free convective boundary layer flow of a nanofluid along a permeable isothermal vertical plate in the presence of heat generation or absorption effects. Matin *et al.* [23] studied magneto-hydrodynamics (MHD) mixed convective flow of nanofluid over a stretching sheet. Magneto-hydrodynamics (MHD) forced convective flow of nanofluid over a horizontal stretching flat plate with variable magnetic field including the viscous dissipation was investigated by Nourazar *et al.* [24]. The effect of a transverse magnetic field on the flow and heat transfer over a stretching surface was examined by Anjali Devi and Thiyagarajan [25].

Despite all the previous work, there is still a lot that is unknown about the flow and heat and mass transfer properties of different nanofluids. For instance, the composition and make of nanoparticles may have an impact on the performance of nanofluid as a heat transfer medium. The aim of the present study is to analyze the effects of Brownian motion parameter and thermophoresis parameter on unsteady boundary layer flow heat and mass transfer of a nanofluid flow past an impulsively stretching surface in the presence of a chemical reaction and an applied magnetic field. The model equations are solved using the spectral relaxation method (SRM) that was recently proposed by Motsa [26]. The spectral relaxation method promises fast convergence with good accuracy, has been successfully used in a limited number of boundary layer flow, heat and mass transfer studies (see [27, 28]). A comparative study for a special case is presented, which shows good agreement with Khan and Pop [6].

2 Governing equations

Consider the two-dimensional unsteady boundary layer flow heat and mass transfer in a nanofluid past an impulsively stretching vertical surface situated at $y = 0$ with stretching

velocity $u(x) = ax$, where a is a constant. The temperature and nanoparticle concentration at the stretching surface are T_w and C_w, respectively, and those of the ambient nanofluid are T_∞ and C_∞, respectively. The x and y directions are taken along and perpendicular to the sheet, respectively. Here we focus mainly in the region $x, y \geq 0$. The Boussinesq approximation is applied here. The continuity, momentum, energy and concentration equations of an unsteady, incompressible nanofluid boundary layer flow are as follows (see Kuznetsov and Nield [8]):

$$\frac{\partial u}{\partial x} + \frac{\partial v}{\partial y} = 0, \tag{1}$$

$$\frac{\partial u}{\partial t} + u\frac{\partial u}{\partial x} + v\frac{\partial u}{\partial y} = \frac{\mu_{nf}}{\rho_{nf}}\frac{\partial^2 u}{\partial y^2} + g\beta_T(T - T_\infty) + g\beta_C(C - C_\infty) - \frac{\sigma B_0^2}{\rho_{nf}}u, \tag{2}$$

$$\frac{\partial T}{\partial t} + u\frac{\partial T}{\partial x} + v\frac{\partial T}{\partial y} = \alpha_{nf}\frac{\partial^2 T}{\partial y^2} + \tau^*\left[D_B\frac{\partial C}{\partial y}\frac{\partial T}{\partial y} + \frac{D_T}{T_\infty}\left(\frac{\partial T}{\partial y}\right)^2\right], \tag{3}$$

$$\frac{\partial C}{\partial t} + u\frac{\partial C}{\partial x} + v\frac{\partial C}{\partial y} = D_B\frac{\partial^2 C}{\partial y^2} + \frac{D_T}{T_\infty}\frac{\partial^2 T}{\partial y^2} - K(C - C_\infty), \tag{4}$$

where u and v are the fluid velocity and normal velocity components along x- and y-directions, respectively; μ_{nf}, ρ_{nf}, σ, B_0, g are the effective dynamic viscosity of the nanofluid, nanofluid density, electrical conductivity, the uniform magnetic field in the y-direction and gravitational acceleration; β_T, β_C, T, C, α_{nf}, τ^* $(= (\rho c)_p/(\rho c)_f)$ are the volumetric thermal expansion coefficient, volumetric solutal expansion coefficient, temperature of fluid in the boundary layer, fluid solutal concentration, the thermal diffusivity of the nanofluid, the ratio of effective heat capacity of the nanoparticle material to heat capacity of the fluid; D_B, D_T, T_∞, K are the Brownian motion coefficient, the thermophoretic diffusion coefficient, mean fluid temperature and the chemical reaction parameter.

The boundary conditions are

$$\begin{aligned} t \geq 0:\quad & u = U_w(x) = ax, \qquad v = 0, \qquad T = T_w, \qquad C = C_w \quad \text{at } y = 0, \\ & T_w(x) = T_\infty + T_0 x, \qquad C_w(x) = C_\infty + C_0 x, \\ t \geq 0:\quad & u, v \to 0, \qquad T \to T_\infty, \qquad C \to C_\infty \quad \text{as } y \to \infty, \end{aligned} \tag{5}$$

and the initial conditions are

$$\begin{aligned} t < 0:\quad & u(x, y, t) = 0, \qquad v(x, y, t) = 0, \\ & T(x, y, t) = T_\infty, \qquad C(x, y, t) = C_\infty, \quad \forall x, y, \end{aligned} \tag{6}$$

where a is the stretching/shrinking rate and stagnation flow rate parameters, with $a < 0$ for shrinking, $a > 0$ for stretching.

The effective dynamic viscosity of the nanofluid was given by Brinkman [29] as

$$\mu_{nf} = \frac{\mu_f}{(1 - \phi)^{2.5}}, \tag{7}$$

where ϕ and μ_f are the solid volume fraction of nanoparticles and the dynamic viscosity of the base fluid.

In equations (1) to (4), the quantities $(\rho c_p)_{nf}$, ρ_{nf} and α_{nf} are given by

$$\begin{aligned}
&(\rho c_p)_{nf} = (1-\phi)(\rho c_p)_f + \phi(\rho c_p)_s,\\
&\rho_{nf} = (1-\phi)\rho_f + \phi\rho_s, \qquad \nu_{nf} = \frac{\mu_{nf}}{\rho_{nf}},\\
&\alpha_{nf} = \frac{k_{nf}}{(\rho c_p)_{nf}}, \qquad \frac{k_{nf}}{k_f} = \frac{(k_s+k_f)-2\phi(k_f-k_s)}{(k_s+k_f)+\phi(k_f-k_s)},
\end{aligned} \tag{8}$$

where ν_{nf}, ρ_{nf}, $(\rho cp)_{nf}$, k_{nf}, k_f, k_s, ρ_s, $(\rho c_p)_f$, $(\rho c_p)_s$ are the nanofluid kinematic viscosity, the electrical conductivity, the nanofluid heat capacitance, thermal conductivity of the nanofluid, thermal conductivity of the fluid, the thermal conductivity of the solid fractions, the density of the solid fractions, the heat capacity of the base fluid, the effective heat capacity of nanoparticles, respectively (see Abu-Nada [30]).

The continuity equation (1) is satisfied by introducing a stream function $\psi(x,y)$ such that

$$u = \frac{\partial\psi}{\partial y}, \qquad v = -\frac{\partial\psi}{\partial x}. \tag{9}$$

Introducing the following non-dimensional variables (see Liao [31]):

$$\begin{aligned}
&\psi = [a\nu_f\xi]^{\frac{1}{2}} x f(\xi,\eta), \quad \xi = 1-\exp(-\tau), \tau = at, \eta = \left[\frac{a}{\nu_f\xi}\right]^{\frac{1}{2}} y,\\
&\theta(\xi,\eta) = \frac{T-T_\infty}{T_w-T_\infty}, \qquad \Phi(\xi,\eta) = \frac{C-C_\infty}{C_w-C_\infty},
\end{aligned} \tag{10}$$

where η, ξ and τ are dimensionless variables and the dimensionless time, $f(\xi,\eta)$ is the dimensionless stream function, $\theta(\xi,\eta)$ is the dimensionless temperature and $\phi(\xi,\eta)$ is the dimensionless solute concentration. By using (10) the governing equations (2) to (4) along with the boundary conditions (5) are reduced to the following two-point boundary value problem:

$$\begin{aligned}
&f''' + \phi_1\left[(1-\xi)\frac{1}{2}\eta f'' + \xi\left(ff'' - f'^2 - Ha^2 f' + Gr_t\theta + Gr_c\phi\right)\right]\\
&\quad = \phi_1\xi(1-\xi)\frac{\partial f'}{\partial\xi},
\end{aligned} \tag{11}$$

$$\begin{aligned}
&\theta'' + \phi_2 Pr\left(\frac{k_f}{k_{nf}}\right)\left[(1-\xi)\frac{1}{2}\eta\theta' + \xi f\theta' + N_b\theta'\phi' + N_T\theta'2\right]\\
&\quad = \phi_2 Pr\left(\frac{k_f}{k_{nf}}\right)(1-\xi)\frac{\partial\theta}{\partial\xi},
\end{aligned} \tag{12}$$

$$\phi'' + Sc\left[(1-\xi)\frac{1}{2}\eta\phi' + \xi f\phi'\right] + \frac{N_T}{N_b}\theta'' - \gamma\xi Sc\phi = Sc\xi(1-\xi)\frac{\partial\phi}{\partial\xi}, \tag{13}$$

subject to the boundary conditions

$$f(\xi,0) = 0, \qquad f'(\xi,0) = 1, \qquad \theta(\xi,0) = 1, \qquad \Phi(\xi,0) = 1, \quad \eta = 0, \xi \geq 0, \tag{14}$$

$$f'(\xi,\infty) = 0, \qquad \theta(\xi,\infty) = 0, \qquad \Phi(\xi,\infty) = 0, \quad \eta \to \infty, \xi \geq 0, \tag{15}$$

where the prime denotes differentiation with respect to η, $\alpha_f = k_f/(\rho c_p)_f$ and $\nu_f = \mu_f/\rho_f$ are the thermal diffusivity and kinetic viscosity of the base fluid, respectively. Other non-dimensional parameters appearing in equations (11) to (13) Ha, Gr_t, Gr_c, Pr, N_b, N_T, Sc, and γ denote the Hartman number, the local temperature Grashof number and the local concentration Grashof number (see Mahdy [32] and Hsiao [33]), the Prandtl number, Brownian motion parameter and thermophoresis parameter (see Khan and Pop [6], Nadeem and Saleem [34]), the Schmidt number and scaled chemical reaction parameter. These parameters are defined mathematically as

$$\begin{aligned} &Ha^2 = \frac{\sigma B_0^2}{a\rho_{nf}}, \qquad Gr_t = \frac{g\beta_T(T_w - T_\infty)}{a^2 x}, \\ &Gr_c = \frac{g\beta_C(C_w - C_\infty)}{a^2 x}, \qquad Pr = \frac{\nu_f}{\alpha_f}, \\ &N_b = \frac{(\rho_c)_p D_B(C_w - C_\infty)}{\nu_f(\rho_p)_f}, \qquad Sc = \frac{\nu_f}{D_B}, \\ &\gamma = \frac{K}{a}, \qquad N_T = \frac{(\rho_c)_p D_T(T_w - T_\infty)}{T_\infty \nu_f(\rho_p)_f}. \end{aligned} \tag{16}$$

The nanoparticle volume fraction parameters ϕ_1 and ϕ_2 are defined as

$$\phi_1 = (1-\phi)^{2.5}\left[1 - \phi + \phi\left(\frac{\rho_s}{\rho_f}\right)\right], \qquad \phi_2 = \left[1 - \phi + \phi\frac{(\rho c)_s}{(\rho c)_f}\right]. \tag{17}$$

2.1 Skin friction, heat and mass transfer coefficients

The skin friction coefficient C_f, the local Nusselt number Nu_x and the local Sherwood number Sh_x characterize the surface drag, wall heat and mass transfer rates, respectively.

The shearing stress at the surface of the wall τ_w is defined as

$$\tau_w = -\mu_{nf}\left(\frac{\partial u}{\partial y}\right)_{y=0} = -\frac{U_w\mu_f}{(1-\phi)^{2.5}x}\sqrt{\frac{U_w x}{\nu_f \xi}}f''(0,\xi), \tag{18}$$

where μ_{nf} is the coefficient of viscosity.

The skin friction coefficient is obtained as

$$C_{fx} = \frac{2\tau_w}{\rho_f U_w^2}, \tag{19}$$

and using equation (18) in (19) we obtain

$$\frac{1}{2}(1-\phi)^{2.5}C_{fx} = -\xi^{-\frac{1}{2}}Re_x^{-\frac{1}{2}}f''(0,\xi). \tag{20}$$

The heat transfer rate at the surface flux at the wall is defined as

$$q_w = -k_{nf}\left(\frac{\partial T}{\partial y}\right)_{y=0} = -k_{nf}\frac{(T_w - T_\infty)}{x}\sqrt{\frac{U_w x}{\nu_f \xi}}\theta'(0,\xi), \tag{21}$$

where k_{nf} is the thermal conductivity of the nanofluid.

The local Nusselt number (heat transfer coefficient) is defined as

$$Nu_x = \frac{xq_w}{k_f(T_w - T_\infty)}. \tag{22}$$

Using equation (21) in equation (22), the dimensionless wall heat transfer rate is obtained as

$$\left(\frac{k_f}{k_{nf}}\right) Nu_x = -\xi^{-\frac{1}{2}} Re_x^{\frac{1}{2}} \theta'(0,\xi). \tag{23}$$

The mass flux at the wall surface is defined as

$$q_m = -D\left(\frac{\partial C}{\partial y}\right)_{y=0} = -D\frac{(C_w - C_\infty)}{x}\sqrt{\frac{U_w x}{\nu_f \xi}}\Phi'(0,\xi), \tag{24}$$

and the local Sherwood number (mass transfer coefficient) is obtained as

$$Sh_x = \frac{xq_m}{D(C_w - C_\infty)}. \tag{25}$$

The dimensionless wall mass transfer rate is obtained as

$$Sh_x = -\xi^{-\frac{1}{2}} Re_x^{\frac{1}{2}} \Phi'(0,\xi), \tag{26}$$

where Re_x represents the local Reynolds number and is defined as

$$Re_x = \frac{xu_\infty}{\nu_f}. \tag{27}$$

3 Cases of special interest

In this section some particular cases of equations (11) to (13) where the equations are reduced to ordinary differential equations are considered.

Case (1): *initial steady-state flow*. For steady flow when $\phi = 0$ (regular fluid), we have $\xi = 0$ corresponding to $t = 0$, thus $f(\eta,0) = f(\eta)$, $\theta(\eta,0) = \theta(\eta)$ and $\Phi(\eta,0) = \Phi(\eta)$. In this case equations (11) to (13) reduce to

$$f''' + \frac{1}{2}\phi_1 \eta f'' = 0, \tag{28}$$

$$\theta'' + \frac{1}{2}\frac{k_f}{k_{nf}} Pr\phi_2 \eta\theta' + \phi_2 \frac{k_f}{k_{nf}} PrN_b\theta'\phi' + \phi_2 \frac{k_f}{k_{nf}} PrN_T\theta' 2 = 0, \tag{29}$$

$$\phi'' + \frac{1}{2} Sc\eta\phi' + \frac{N_T}{N_b}\theta'' = 0, \tag{30}$$

subject to the boundary conditions

$$\begin{aligned} &f(0) = 0, \qquad f'(0) = 1, \qquad \theta(0) = 1, \qquad \Phi(0) = 1, \\ &f'(\infty) = 0, \qquad \theta(\infty) = 0, \qquad \Phi(\infty) = 0, \end{aligned} \tag{31}$$

where prime denotes differentiation with respect to η. Equation (28) subject to the boundary conditions (31) admits the exact solution (see Liao [31])

$$f(\eta) = \eta\left(1 - \operatorname{erf}\left(\frac{\eta}{2}\right)\right) + \frac{2}{\sqrt{\pi}}\left(1 - \exp^{(-\eta^2/4)}\right), \tag{32}$$

where $\operatorname{erf}(\nu)$ is the error function defined as

$$\operatorname{erf}(\nu) = \frac{2}{\sqrt{\pi}}\int_0^{\nu} e^{-z^2}\,dz. \tag{33}$$

Case (2): *final steady-state flow*. In this case, we have $\xi = 1$ ($t \to \infty$), corresponding to $f(\eta,1) = f(\eta)$, $\theta(\eta,1) = \theta(\eta)$ and $\phi(\eta,1) = \phi(\eta)$.

Equations (11) to (13) reduce to the following forms:

$$f''' + ff'' - f'^2 + 1 - Ha^2 f' + Gr_t\theta + Gr_c\phi = 0, \tag{34}$$

$$\theta'' + \frac{k_f}{k_{nf}}Pr\phi_2\left(f\theta' + N_b\theta'\phi'\right) + \frac{k_f}{k_{nf}}PrN_T\theta'^2 = 0, \tag{35}$$

$$\phi'' + Sc\left(f\phi' - \gamma\phi + \frac{N_T}{N_b}\theta''\right) = 0, \tag{36}$$

subject to the boundary conditions (31). Equations (11) to (13) were solved using the SRM, Motsa [26]. The SRM is an iterative procedure that employs the Gauss-Seidel type of relaxation approach to linearize and decouple the system of differential equations. Further details of the rules of the SRM can be found in [27, 28]. The linear terms in each equation are evaluated at the current iteration level (denoted by $r+1$) and nonlinear terms are assumed to be known from the previous iteration level (denoted by r). The linearized form of (11) to (13) is

$$f'''_{r+1} + a_{1,r}f''_{r+1} + a_{2,r}f'_{r+1} - \phi_1\xi(1-\xi)\frac{\partial f'}{\partial\xi} = R_{1,r}, \tag{37}$$

$$\theta''_{r+1} + b_{1,r}\theta'_{r+1} - \frac{k_f}{k_{nf}}Pr\phi_2\xi(1-\xi)\frac{\partial\theta}{\partial\xi} = R_{2,r}, \tag{38}$$

$$\phi''_{r+1} + c_{r,1}\phi'_{r+1} + c_{2,r}\phi_{r+1} - Sc\xi(1-\xi)\frac{\partial\phi}{\partial\xi} = R_{3,r}, \tag{39}$$

where

$$a_{1,r} = \phi_1\left[\frac{\eta}{2}(1-\xi) + \xi f_r\right], \qquad a_{2,r} = -\phi_1\xi Ha^2,$$

$$R_{1,r} = -\phi_1\xi\left[Gr_t\theta_r + Gr_c\phi_r - f'^2_r\right],$$

$$b_{1,r} = \frac{k_f}{k_{nf}}Pr\phi_2\left[\frac{\eta}{2}(1-\xi) + \xi f_{r+1} + N_b\phi'_{r+1}\right], \qquad R_{2,r} = -\frac{k_f}{k_{nf}}Pr\phi_2\xi N_T\theta'^2_r,$$

$$c_{1,r} = \frac{\eta}{2}(1-\xi)Sc + Sc\xi f_{r+1}, \qquad c_{2,r} = -Sc\xi\gamma,$$

$$R_{3,r} = -\frac{N_T}{N_b}\theta''_{r+1}.$$

It must be noted that equations (37)-(39) are now linear and, being decoupled, can be solved sequentially to obtain approximate solutions for $f(\eta,\xi)$, $\theta(\eta,\xi)$ and $\phi(\eta,\xi)$. In this study, the Chebyshev spectral collocation method was used to discretize in η and finite differences with central differencing for derivatives was used to discretize in ξ. Starting from initial guesses for f, θ and ϕ, equations (37)-(39) were solved iteratively until the approximate solutions converged within a certain prescribed tolerance level. The accuracy of the results was validated against results from literature for some special cases of the governing equations.

4 Results and discussion

The nonlinear boundary value problem (11) to (13) subject to the boundary conditions (14) and (15) cannot be solved in closed form, so these equations are solved numerically using the spectral relaxation method (SRM) for Cu-water and Ag-water nanofluids for $0 \leq \xi \leq 1$. The thermophysical properties of the nanofluids used in the numerical simulations are given in Table 1. Extensive calculations have been performed to obtain the velocity, temperature, concentration profiles as well as skin friction, the local Nusselt number and the local Sherwood number for various values of physical parameters such as ϕ, Ha, Gr_t, Gr_c, Pr, N_b, N_T, Sc and γ.

To determine the accuracy of our numerical results, the heat and the mass transfer coefficients are compared with the published results of Khan and Pop [6] in Tables 2 and 3. Here, we have varied the N_T with N_b while keeping other physical parameters fixed. Ta-

Table 1 Thermophysical properties of the base fluid and the nanoparticles [35] and [36]

Physical properties	Base fluid (water)	Copper (Cu)	Silver (Ag)
C_p (J/kgK)	4,179	385	235
ρ (Kg/m^3)	997.1	8,933	10,500
k (W/mK)	0.613	401	429
$\alpha \times 10^7$ (m^2/s)	1.47	1,163.1	1,738.6
$\beta \times 10^5$ (K^{-1})	21	1.67	1.89

Table 2 Comparison of values of $-\theta'(0,\xi)$ for various values of N_T and N_b with $\phi = 0$ (regular fluid), $Ha = Gr_t = Gr_c = \gamma = 0$, $\xi = 1$, $Pr = 10$, $Sc = 10$

N_T	$N_b = 0.1$		$N_b = 0.2$		$N_b = 0.3$	
	[6]	Present results	[6]	Present results	[6]	Present results
0.1	0.9524	0.9519	0.5056	0.5052	0.2522	0.2522
0.2	0.6932	0.6930	0.3654	0.3662	0.1816	0.1841
0.3	0.5201	0.5219	0.2731	0.2760	0.1355	0.1394
0.4	0.4026	0.4040	0.2110	0.2117	0.1046	0.1044
0.5	0.3211	0.3185	0.1681	0.1639	0.0833	0.0779

Table 3 Comparison of values of $-\phi'(0,\xi)$ for various values of N_T and N_b with $\phi = 0$ (regular fluid), $Ha = Gr_t = Gr_c = \gamma = 0$, $\xi = 1$, $Pr = 10$, $Sc = 10$

N_T	$N_b = 0.1$		$N_b = 0.2$		$N_b = 0.3$	
	[6]	Present results	[6]	Present results	[6]	Present results
0.1	2.1294	2.1294	2.3819	2.3817	2.4100	2.4097
0.2	2.2740	2.2745	2.5152	2.5145	2.5150	2.5134
0.3	2.5286	2.5242	2.6555	2.6513	2.6088	2.6047
0.4	2.7952	2.7883	2.7818	2.7787	2.6876	2.6862
0.5	3.0351	3.0413	2.8883	2.8944	2.7519	2.7574

Table 4 Comparison of the SRM solutions for $f''(\xi,0)$, $-\theta'(\xi,0)$, and $-\phi'(\xi,0)$ against those of the SQLM at different values of ξ, $N_T = 0.1$, $N_b = 0.1$, $Pr = 7$, $Gr_t = 0.1$, $Gr_c = 0.1$, $Sc = 1$, $\phi = 0.2$, $\gamma = 2$, $Ha = 3$

ξ	$f''(\xi,0)$		$-\theta'(\xi,0)$		$-\phi'(\xi,0)$	
	SRM	SQLM	SRM	SQLM	SRM	SQLM
0.1	−1.024404	−1.024404	0.861024	0.861024	0.372386	0.372386
0.2	−1.062742	−1.062742	0.864900	0.864900	0.389380	0.389380
0.3	−1.088333	−1.088333	0.872739	0.872739	0.386305	0.386305
0.4	−1.108200	−1.108200	0.882753	0.882753	0.372517	0.372517
0.5	−1.124261	−1.124261	0.894651	0.894651	0.350129	0.350129
0.6	−1.136890	−1.136890	0.908632	0.908632	0.318838	0.318838
0.7	−1.145390	−1.145390	0.925350	0.925350	0.276272	0.276272
0.8	−1.146964	−1.146964	0.946411	0.946411	0.216141	0.216141
0.9	−1.127531	−1.127531	0.977047	0.977047	0.118365	0.118365
1.0	−4.252384	−4.252384	1.495226	1.495226	0.463421	0.463421

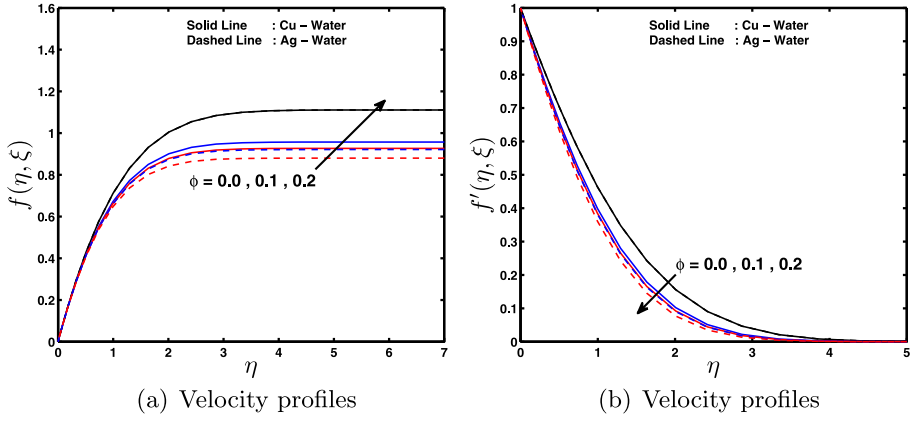

(a) Velocity profiles (b) Velocity profiles

Figure 1 Effect of various nanoparticle values fraction ϕ on (a) and (b) for $Gr_t = 0.2$, $Ha = 0.2$, $Gr_c = 0.2$, $N_T = 0.01$, $Pr = 7$, $N_b = 0.01$, $\gamma = 1$, $Sc = 1$ and $\xi = 0.5$.

bles 2 and 3 give a comparison of the SRM results with those obtained by Khan and Pop [6] when $Ha = Gr_t = Gr_c = \gamma = \phi = 0$, $Pr = 10$, $Sc = 10$ and $\xi = 1$ for different values of the Brownian motion and thermophoresis parameters. It is observed that the present results are in good agreement with results in the literature. In Table 4, approximate solutions of the skin friction coefficient, surface heat transfer and surface mass transfer rates at different values of flow parameters are presented and compared with the SQLM solutions. Values of the skin friction coefficient, reduced Nusselt and Sherwood numbers at different values of ξ are presented in Table 4. The table also shows a comparison of the SHAM and SQLM results. As can be seen from the table, the results match perfectly well for the set accuracy level.

The effects of physical parameters on various fluid dynamic quantities are show in Figures 1-11.

Figures 1-4 illustrate the effect of the nanoparticle volume fraction ϕ on the velocity, temperature and concentration profiles, respectively, in the case of a Cu-water nanofluid. It is clear that as the nanoparticle volume fraction increases, the nanofluid velocity and the temperature profile increase while the opposite trend is observed for the concentration profile. Increasing the volume fraction of nanoparticles increases the thermal conductivity of the nanofluid, and we observe that thickening of the thermal boundary layer and the

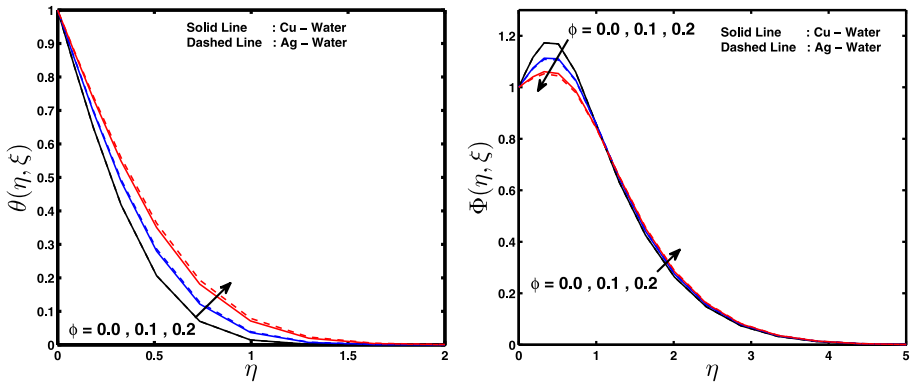

(a) Temperature profiles (b) Concentration profiles

Figure 2 Effect of various nanoparticle values fraction ϕ on (a) and (b) for $Gr_t = 0.2$, $Ha = 0.2$, $Gr_c = 0.2$, $N_T = 0.01$, $Pr = 7$, $N_b = 0.01$, $\gamma = 1$, $Sc = 1$ and $\xi = 0.5$.

Figure 3 Effect of various nanoparticle values fraction ϕ on skin friction coefficient for $Gr_t = 0.2$, $Ha = 0.2$, $Gr_c = 0.2$, $N_T = 0.01$, $Pr = 7$, $N_b = 0.01$, $\gamma = 1$ and $Sc = 1$.

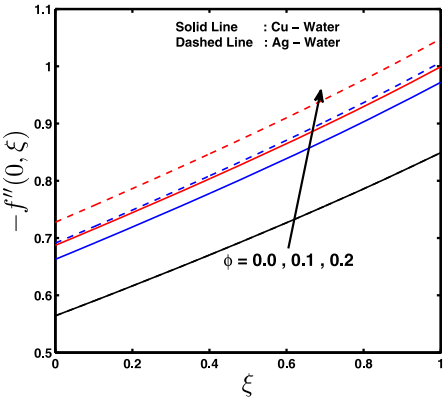

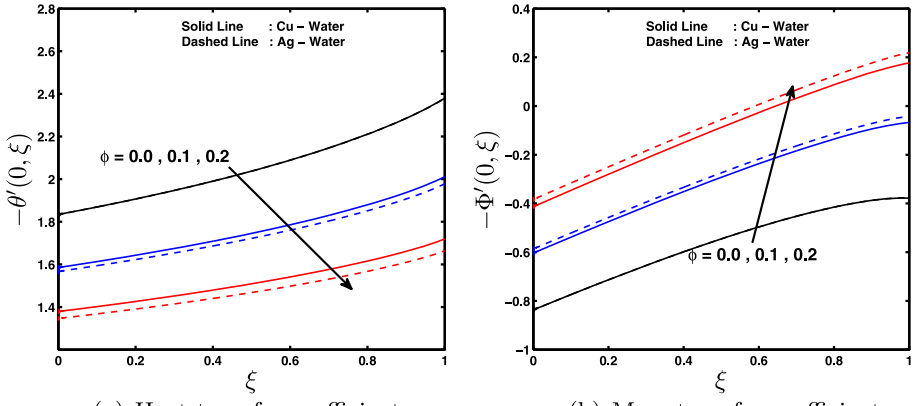

(a) Heat transfer coefficient (b) Mass transfer coefficient

Figure 4 Effect of various nanoparticle values fraction ϕ on (a) and (b) for $Gr_t = 0.2$, $Ha = 0.2$, $Gr_c = 0.2$, $N_T = 0.01$, $Pr = 7$, $N_b = 0.01$, $\gamma = 1$ and $Sc = 1$.

velocity in the case of an Ag-water nanofluid are relatively less than in the case of a Cu-water. We also note that since the conductivity of silver is higher than that of copper, the temperature distribution in the Ag-water nanofluid is higher than that in the Cu-water nanofluid. With increase in the nanoparticle volume fraction, the concentration boundary layer thickness increases for both types of nanofluids considered, and the opposite trend is observed when the concentration profile decreases.

Figure 3 shows that the skin friction coefficient $-f''(0,\xi)$ increases monotonically with increasing ξ. The result is true for both types of nanofluids. The minimum value of the skin friction in the case of the Cu-water nanofluid is achieved at a smaller value of ξ in comparison with the Ag-water nanofluid. Furthermore, in this paper it is found that the Ag-water nanofluid shows higher drag as compared to the Cu-water nanofluid. The dimensionless wall heat transfer rate and the dimensionless wall mass transfer rate are shown as functions of ξ in Figure 4(a) and (b), respectively. We observe that the wall heat transfer rate $-\theta'(0,\xi)$ decreases, while the opposite trend is observed in the case of the wall mass transfer rate $-\Phi'(0,\xi)$. The Cu-water nanofluid exhibits higher wall heat transfer rate as compared to the Ag-water nanofluid, while the opposite trend is observed for the wall mass transfer rate. The presence of nanoparticle tends to increase the wall heat transfer rate and to decrease the wall mass transfer rate with increasing the values of dimensionless variable ξ.

Figures 5-7 show the influence of the Hartman number on the velocity, temperature, skin friction coefficient $-f''(0,\xi)$, the local Nusselt number $-\theta'(0,\xi)$ and the local Sherwood number $-\Phi'(0,\xi)$. The effect of Hartman number *Ha* is to decrease the nanofluid velocity and the wall heat transfer coefficient, whereas it increases the skin friction coefficient and the wall mass transfer coefficient. A similar observation was made by Haroun *et al.* [11]. The momentum boundary layer thickness decreases with increase in the Hartman number. In the case of the Cu-water nanofluid it is relatively higher than that of the Ag-water nanofluid for nanofluid velocity. Figure 6 shows the skin friction coefficient as a function of ξ. It is clear that for the Cu-water nanofluid and the Ag-water nanofluid, the skin friction coefficient increases when ξ increases. We note that the Ag-water nanofluid exhibits higher drag to the flow as compared to the Cu-water nanofluid. Figure 7 shows the wall heat and mass transfer rates for different values of the Hartman number *Ha*, it is clear that the value of wall heat transfer rate decreases when ξ increases, in the case of

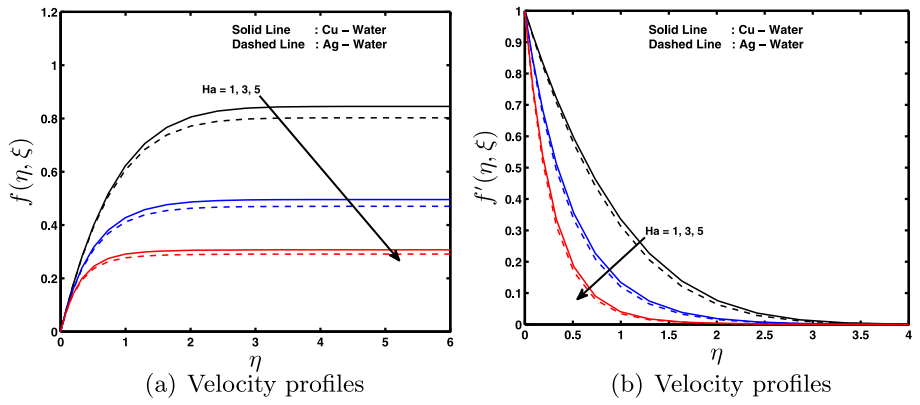

(a) Velocity profiles (b) Velocity profiles

Figure 5 Effect of various values of the Hartman number *Ha* on (a) and (b) for $Gr_t = 0.2$, $\phi = 0.2$, $Gr_c = 0.2$, $N_T = 0.01$, $Pr = 7$, $N_b = 0.01$, $\gamma = 1$, $Sc = 1$ and $\xi = 0.5$.

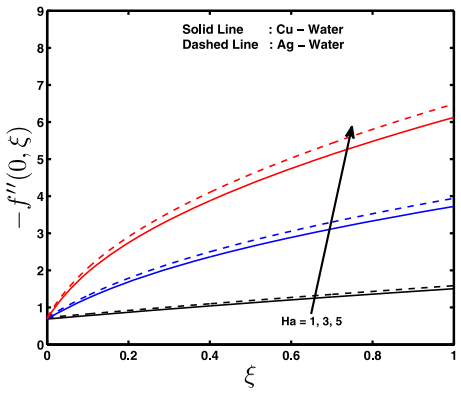

Figure 6 Effect of various values of the Hartman number *Ha* on skin friction coefficient for $Gr_t = 0.2$, $\phi = 0.2$, $Gr_c = 0.2$, $N_T = 0.01$, $Pr = 7$, $N_b = 0.01$, $\gamma = 1$ and $Sc = 1$.

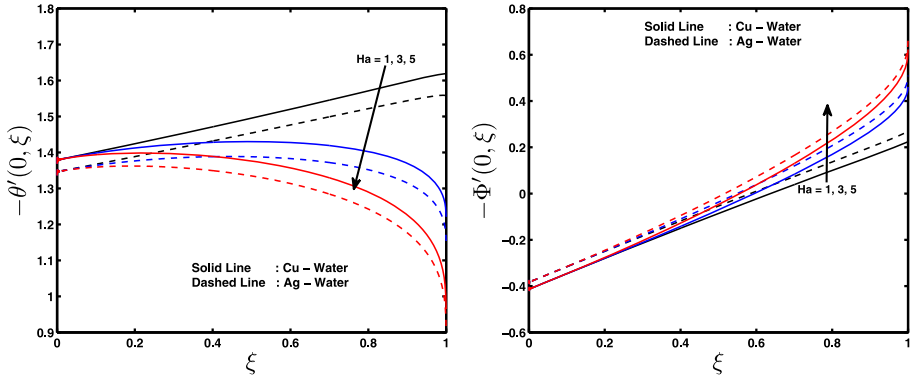

(a) Heat transfer coefficient (b) Mass transfer coefficient

Figure 7 Effect of various values of the Hartman number *Ha* on (a) and (b) for $Gr_t = 0.2$, $\phi = 0.2$, $Gr_c = 0.2$, $N_T = 0.01$, $Pr = 7$, $N_b = 0.01$, $\gamma = 1$ and $Sc = 1$.

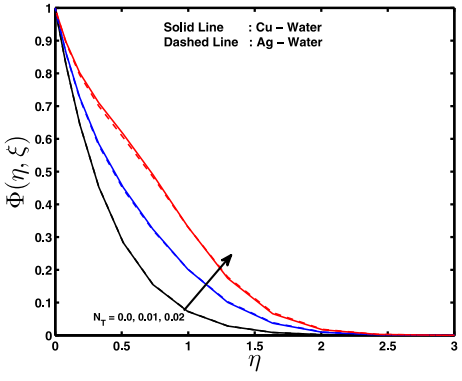

Figure 8 Effect of thermophoretic parameter N_T on concentration profiles for $Gr_t = 0.2$, $\phi = 0.2$, $Gr_c = 0.2$, $Ha = 2$, $Pr = 7$, $N_b = 0.01$, $\gamma = 4$, $Sc = 1$ and $\xi = 0.5$.

the Ag-water nanofluid it is less than that in the case of the Cu-water nanofluid. Further, the wall mass transfer rate increases when ξ increases, we observe that in the case of a Cu-water nanofluid it is less than that of an Ag-water nanofluid.

Figures 8 to 9 show the effect of the thermophoretic parameter N_T on the concentration profile, wall heat and mass transfer rates, respectively. In the case of a Cu-water nanofluid and an Ag-water nanofluid the concentration profile increases and the wall heat and mass

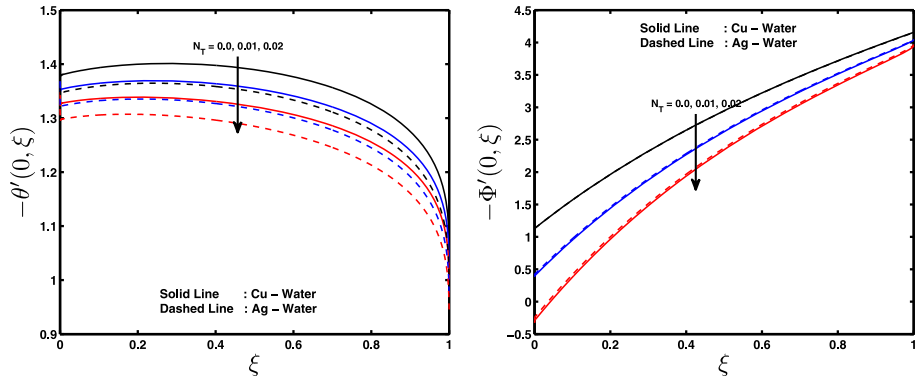

Figure 9 Effect of thermophoretic parameter N_T on (a) and (b) for $Gr_t = 0.2$, $\phi = 0.2$, $Gr_c = 0.2$, $Ha = 4$, $Pr = 7$, $N_b = 0.01$, $\gamma = 4$ and $Sc = 4$.

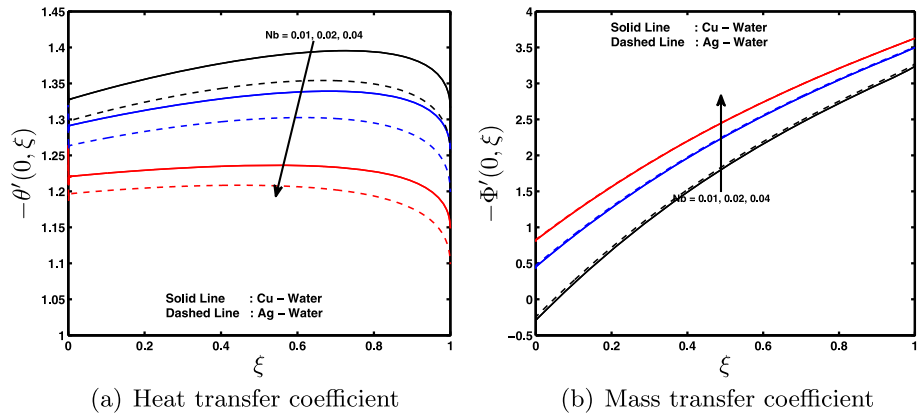

Figure 10 Effect of Brownian motion parameter N_b on (a) and (b) for $Gr_t = 0.2$, $\phi = 0.2$, $Gr_c = 0.2$, $Ha = 2$, $Pr = 7$, $N_T = 0.02$, $\gamma = 3$ and $Sc = 4$.

transfer rates decrease with an increase in the thermophoretic parameter. It is observed that the concentration profile and the wall heat transfer rate in the case of the Ag-water nanofluid are less than those of the Cu-water nanofluid, while the opposite trend is observed in the case of the wall mass transfer rate. We found that the wall heat transfer rate got higher value when $\xi = 0$, and then the opposite trend is observed when $\xi = 1$. The mass transfer rate got less value when $\xi = 0$, while in the case $\xi = 1$ it got the higher value. The fast flow from the stretching sheet carries with it nanoparticles leading to an increase in the mass volume fraction boundary layer thickness.

Figure 10(a) and (b) shows the effect of the Brownian motion parameter N_b on the wall heat and mass transfer rates. Figure 10(a) shows that the heat transfer rate decreases with increasing N_b. The mass transfer at the wall increases with the increase in N_b. The heat transfer rate for the Cu-water nanofluid is higher than that for the Ag-water nanofluid, while the opposite is true for the mass transfer rate (see Figure 10).

Figure 11(a) and (b) shows the impact of the Soret number on the concentration profiles and the mass transfer coefficient, where the concentration profiles grow less while the mass transfer coefficient increases with an increase in the Soret number. Again, Fig-

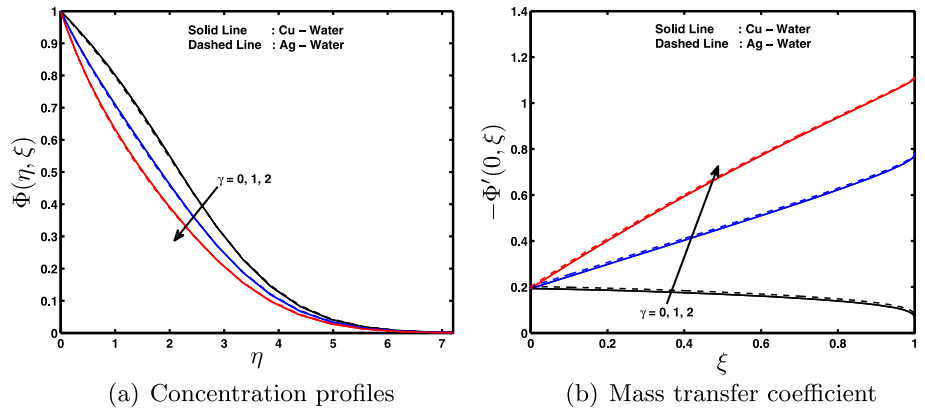

(a) Concentration profiles (b) Mass transfer coefficient

Figure 11 Effect of chemical reaction parameter γ on concentration profiles and the local Sherwood number for $Gr_t = 0.2$, $\phi = 0.2$, $Gr_c = 0.2$, $Ha = 2$, $Pr = 7$, $N_T = 0.01$, $N_b = 0.01$, $Sc = 0.6$ and $\xi = 0.5$.

ure 11(a) and (b) shows that as the Soret number increases, the boundary layer thickness for the solute concentration reduces. The mass transfer coefficient is increasing when the Soret number is positive.

5 Conclusions

We have investigated the heat and mass transfer in unsteady MHD boundary layer flow in nanofluid due to an impulsively stretching surface with chemical reaction and an applied magnetic field. Other parameters of interest in this study included the Brownian motion parameter and thermophoresis parameter. In this paper we considered Cu-water and Ag-water nanofluids and assumed that the nanoparticle volume fraction can be actively controlled at the boundary surface. We have solved the model equations using the spectral relaxation method, and to benchmark our solutions we compared our results with some limiting cases from the literature. These results were found to be in a good agreement. From the numerical simulations, some results can be drawn as follows:

(i) The velocity profiles increase with increase in the nanoparticle volume fraction, while the opposite trend is observed with increase in the value of the Hartman number.

(ii) The temperature profiles increase with increasing nanoparticle volume fraction values.

(iii) The skin friction decreases with an increase in the values of the nanoparticle volume fraction, while the opposite trend is observed for increasing values of the Hartman number.

(iv) The heat transfer coefficient decreases with increase in the values of the nanoparticle volume fraction, the Hartman number, thermophoretic and Brownian motion parameters.

(v) The mass transfer coefficient increases with an increase in the nanoparticle volume fraction, chemical reaction parameter, Hartman number and Brownian motion parameter, while the opposite trend is observed for increasing values of the thermophoretic parameter.

Abbreviations

t: time; p: pressure; a: positive constant; q_w: wall heat flux; q_m: wall mass flux; Pr: Prandtl number; Sc: Schmidt number; Ha: Hartman number; N_T: thermophoresis parameter; N_b: Brownian motion parameter; Sh_x: local Sherwood number; Re_x: local Reynolds number; Nu_x: local Nusselt number; Gr_t: local temperature Grashof number; Gr_c: local concentration Grashof number; k_{nf}: thermal conductivity of nanofluid; C_{fx}: skin friction coefficient; $f(\xi, \eta)$: dimensionless stream function; T_∞: ambient temperature; C_∞: ambient concentration; g: acceleration due to gravity; B_0: uniform magnetic field; u, v: velocity components along x, y directions; x: coordinate along the sheet; y: coordinate normal to the sheet; T: local fluid temperature; T_w: temperature at the stretching surface; D_B: Brownian motion coefficient; D_T: thermophoretic diffusion coefficient; C: solutal concentration; C_s: concentration susceptibility; C_w: concentration at the stretching surface; v_w: prescribed suction velocity; K: chemical reaction parameter; k_s: solid volume fraction; k_f: thermal conductivity of fluid. *Greek symbols*: ρ_{nf}: nanofluid density; ν_{nf}: nanofluid kinematic viscosity; μ_{nf}: coefficient of viscosity; $(\rho cp)_{nf}$: nanofluid heat capacitance; α_{nf}: thermal diffusivity of nanofluid; μ_{nf}: effective dynamic viscosity nanofluid; $(cp)_{nf}$: specific heat of fluid at constant pressure; τ_w: shearing stress at the surface of the wall; γ: scaled chemical reaction parameter; σ: electrical conductivity; ϕ: fraction of nanoparticles; ϕ_1, ϕ_2: nanoparticle volume fraction; $\psi(x, y)$: dimensionless stream function; $(\rho c_p)_f$: heat capacity of base fluid; ρ_f: density of base fluid; μ_f: dynamic viscosity of fluid; ϕ: fraction of nanoparticles; ρ_s: density of solid fractions; β_C: volumetric solutal expansion coefficient; β_T: volumetric thermal expansion coefficient; $(\rho c_p)_s$: effective heat capacity of nanoparticle. *Subscripts*: f: fluid; nf: nanofluid; s: solid.

Competing interests

The authors have declared that they have no competing interests.

Authors' contributions

All authors contributed equally to the writing of this paper. All authors read and approved the final manuscript.

Author details

[1]School of Mathematics, Statistics and Computer Science, University of KwaZulu-Natal, Private Bag X01, Scottsville, Pietermaritzburg, 3209, South Africa. [2]Shanghai Key Lab of Vehicle Aerodynamics and Vehicle Thermal Management Systems, Tongji University, 4800 Cao An Rd., Jiading, Shanghai, 201804, China.

Received: 29 May 2015 Accepted: 25 August 2015 Published online: 15 September 2015

References

1. Choi, SUS: Enhancing thermal conductivity of fluids with nanoparticles. In: The Proceedings of the ASME International Mechanical Engineering Congress and Exposition (San Francisco, USA, ASME, FED, 231/MD), vol. 66, pp. 99-105 (1995)
2. Isha, A, Nazar, R, Pop, I: Hydromagnetic flow and heat transfer adjacent to a stretching vertical sheet. Heat Mass Transf. **44**, 921-927 (2008)
3. Mahapatra, TR, Mondal, S, Pal, D: Heat transfer due to magnetohydrodynamic stagnation-point flow of a power-law fluid towards a stretching surface in the presence of thermal radiation and suction/injection. ISRN Thermodyn. **2012**, Article ID 465864 (2012)
4. Das, SK, Cho, SUS, Yu, W, Pradeep, T: Nanofluids: Science and Technolog. Wiley, New York (2007)
5. Buongiorno, J: Convective transport in nanofluids. J. Heat Transf. **128**, 240-250 (2006)
6. Khan, WA, Pop, I: Boundary layer flow of a nanofluid past a stretching sheet. Int. J. Heat Mass Transf. **53**, 2477-2483 (2010)
7. Hady, FM, Ibrahim, FS, Abdel-Gaied, SM, Mohamed, R: Radiation effect on viscous flow of a nanofluid and heat transfer over a nonlinearly stretching sheet. Nanoscale Res. Lett. **7**, 229 (2012)
8. Kuznetsov, AV, Nield, DA: Natural convective boundary layer flow of a nanofluid past a vertical plate. Int. J. Therm. Sci. **49**, 243-247 (2010)
9. Nield, DA, Kuznetsov, AV: The Cheng-Minkowycz problem for natural convective boundary layer flow in a porous medium saturated with a nanofluid. Int. J. Heat Mass Transf. **52**, 5792-5795 (2009)
10. Yacob, NA, Ishak, A, Pop, I, Vajravelu, K: Boundary layer flow past a stretching/shrinking surface beneath an external uniform shear flow with a convective surface boundary condition in a nanofluid. Nanoscale Res. Lett. **6**, 314 (2011). doi:10.1186/1556-276X-6-314
11. Haroun, NAH, Sibanda, P, Mondal, S, Motsa, SS: On unsteady MHD mixed convection in a nanofluid due to a stretching/shrinking surface with suction/injection using the spectral relaxation method. Bound. Value Probl. **2015**, 24 (2015). doi:10.1186/s13661-015-0289-5
12. Hamad, MAA, Ferdows, M: Similarity solution of boundary layer stagnation point flow towards a heated porous stretching sheet saturated with a nanofluid with heat absorption/generation and suction/blowing. Commun. Nonlinear Sci. Numer. Simul. **17**, 132-140 (2012)
13. Rashidi, MM, Erfani, E: The modified differential transform method for investigating nano boundary-layers over stretching surfaces. Int. J. Numer. Methods Heat Fluid Flow **21**, 864-883 (2011)
14. Rashidi, MM, Freidoonimehr, N, Hosseini, A, Anwar Bég, O, Hung, TK: Homotopy simulation of nanofluid dynamics from a non-linearly stretching isothermal permeable sheet with transpiration. Meccanica **49**, 469-482 (2014)
15. Anwar Bég, O, Rashidi, MM, Akbari, M, Hosseini, A: Comparative numerical study of single-phase and two-phase models for bio-nanofluid transport phenomena. J. Mech. Med. Biol. **14**, 1450011 (2014)
16. Garoosi, F, Jahanshaloo, L, Rashidi, MM, Badakhsh, A, Ali, MA: Numerical simulation of natural convection of the nanofluid in heat exchangers using a Buongiorno model. Appl. Math. Comput. **254**, 183-203 (2015)
17. Mălin, M: Multiple solutions for a class of oscillatory discrete problems. Adv. Nonlinear Anal. (2015). doi:10.1515/anona-2015-0027
18. Mălin, M: Emden-Fowler problem for discrete operators with variable exponent. Electron. J. Differ. Equ. **2014**, 55 (2014)
19. Kleinstreuer, C, Li, J, Koo, J: Microfluidics of nano-drug delivery. Int. J. Heat Mass Transf. **51**, 5590-5597 (2008)

20. Capretto, L, Cheng, W, Hill, M, Zhang, X: Micromixing within microfluidic devices. Top. Curr. Chem. **304**, 27-68 (2011)
21. Yazdi, MH, Abdullah, S, Hashim, I, Sopian, K: Slip MHD liquid flow and heat transfer over non-linear permeable stretching surface with chemical reaction. Int. J. Heat Mass Transf. **54**, 3214-3225 (2011)
22. Chamkha, AJ, Aly, AM: MHD free convection flow of a nanofluid past a vertical plate in the presence of heat generation or absorption effects. Chem. Eng. Commun. **198**, 425-441 (2011)
23. Matin, MH, Nobari, MRH, Jahangiri, P: Entropy analysis in mixed convection MHD flow of nanofluid over a non-linear stretching sheet. J. Therm. Sci. Techonol. **7**(1), 104-119 (2012)
24. Nourazar, SS, Matin, MH, Simiari, M: The HPM applied to MHD nanofluid flow over a horizontal stretching plate. J. Appl. Math. **2011**, Article ID 876437 (2011). doi:10.1155/2011/876437
25. Anjali Devi, SP, Thiyagarajan, M: Steady nonlinear hydromagnetic flow and heat transfer over a stretching surface of variable temperature. Heat Mass Transf. **42**, 671-677 (2006)
26. Motsa, SS: A new spectral relaxation method for similarity variable nonlinear boundary layer flow systems. Chem. Eng. Commun. **201**, 241-256 (2014)
27. Motsa, SS, Dlamini, PG, Khumalo, M: Spectral relaxation method and spectral quasilinearization method for solving unsteady boundary layer flow problems. Adv. Math. Phys. **2014**, Article ID 341964 (2014). doi:10.1155/2014/341964
28. Motsa, SS, Makukula, ZG: On spectral relaxation method approach for steady von Karman flow of a Reiner-Rivlin fluid with Joule heating and viscous dissipation. Cent. Eur. J. Phys. **11**, 363-374 (2013)
29. Brinkman, HC: The viscosity of concentrated suspensions and solution. J. Chem. Phys. **20**, 571-581 (1952)
30. Abu-Nada, E: Application of nanofluids for heat transfer enhancement of separated flows encountered in a backward facing step. Int. J. Heat Fluid Flow **29**, 242-249 (2008)
31. Liao, SJ: An analytic solution of unsteady boundary layer flows caused by an impulsively stretching plate. Commun. Nonlinear Sci. Numer. Simul. **11**, 326-329 (2006)
32. Mahdy, A: Unsteady mixed convection boundary layer flow and heat transfer of nanofluids due to stretching sheet. Nucl. Eng. Des. **249**, 248-255 (2012)
33. Hsiao, KL: Nanofluid flow with multimedia physical features for conjugate mixed convection and radiation. Comput. Fluids **104**, 1-8 (2014)
34. Nadeem, S, Saleem, S: Analytical study of third grade fluid over a rotating vertical cone in the presence of nanoparticles. Int. J. Heat Mass Transf. **85**, 1041-1048 (2015)
35. Sheikholeslami, M, Bandpy, MG, Ganji, DD, Soleimani, S, Seyyedi, SM: Natural convection of nanofluids in an enclosure between a circular and a sinusoidal cylinder in the presence of magnetic field. Int. Commun. Heat Mass Transf. **39**, 1435-1443 (2012)
36. Oztop, HF, Abu-Nada, E: Numerical study of natural convection in partially heated rectangular enclosures filled with nanofluids. Int. J. Heat Fluid Flow **29**, 1326-1336 (2008)